MNRAS 000, 1–2 (2020) Preprint February 26, 2020 Compiled using MNRAS LaTeX style file v3.0

Kinematics of the Turtle Nebula (Will's part)

William J. Henney*
Instituto de Radioastronomía y Astrofísica, Universidad Nacional Autónoma de México, Apartado Postal 3-72, 58090 Morelia, Michaoacán, Mexico

Accepted XXX. Received YYY; in original form ZZZ

ABSTRACT
Material to be incorporated into the main paper by Teresa.

Key words: Atomic physics – Radiative transfer – Photodissociation regions

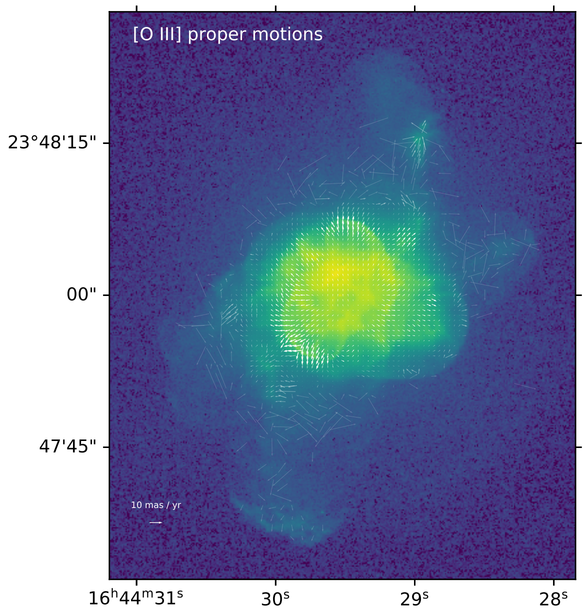

Figure 1. Proper motions derived from two HST [O III] images (F502N filter) separated by 10.45 years, using the FLCT algorithm with a Gaussian window width of 10 pixels. The key at bottom left shows a proper motion of 10 mas yr^{-1}, corresponding to 95 km s^{-1} for an assumed distance of 2 kpc.

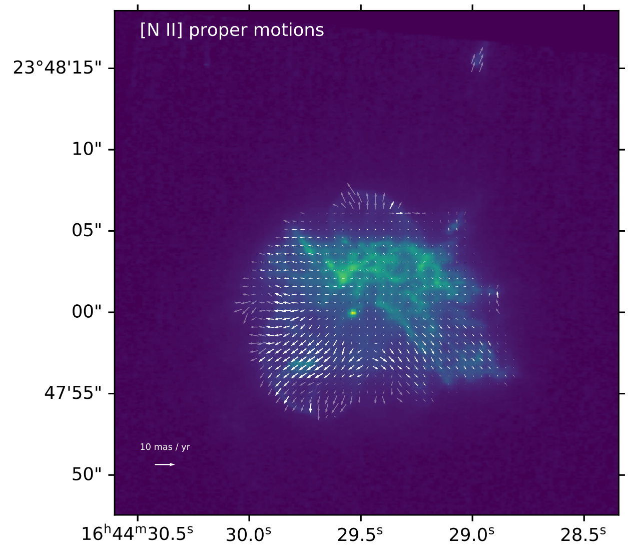

Figure 2. As Fig. 1 but for two HST [N II] images (F658N filter). Note that the field of view is cropped slightly smaller than for [O III].

1 INTRODUCTION

2 OBSERVATIONS AND DATA REDUCTION

3 LONGSLIT SPECTROSCOPY

4 PROPER MOTIONS

Proper motions are calculated from HST WFPC2 imaging at two epochs separated by approximately 10 years, using the FLCT method (Welsch et al. 2004; Fisher & Welsch 2008).[1] Results are shown in Figures 1 and 2 for [O III] and [N II], respectively. In both cases, the images were remapped to a uniform square pixel grid at the WFC resolution of 0.1 arcsec pix^{-1} before applying the algorithm. The resultant per-pixel motions between the two epochs are found to be of order 0.5 pix ($\approx$ 5 mas yr^{-1}) and these raw re-

[1] We used version 1.07 of FLCT, obtained from http://cgem.ssl.berkeley.edu/cgi-bin/cgem/FLCT/home, together with version 1.04 of the Python wrapper pyflct, obtained from https://github.com/PyDL/pyflct.

* w.henney@irya.unam.mx

sults were then corrected by applying a global shift to force the motion of the central star to be zero. The systematic error from the global alignment of the two epochs is estimated to be 1.5 mas yr^{-1}, which is expected to dominate the proper motion uncertainties in the brighter parts of the nebula. In fainter and more featureless regions of the nebula, the proper motions are increasingly affected by random noise, which can be seen in parts of the lobes in Figure 1.

The corrected results, as shown in the figures, can be seen to display motions that are predominantly radial from the central star. To convert the angular motions into transverse velocities, we assume a distance of 2 kpc, so that 10 mas yr^{-1} is equivalent to 95 km s^{-1}. From the [O III] images (Fig. 1), the fastest plane-of-sky motions are of order 60 km s^{-1}, and are chiefly along the NNW–SSE direction, including the projected major axis of the inner peanut shell, the NW knot, the N jet, and the end-cap of the S lobe. Motions along the perpendicular ENE–WSW direction are typically slower, of order 30 km s^{-1}. Note that proper motions are unavailable for the end cap of the N lobe since the second epoch HST image does not cover this region.

The [N II] images (Fig. 2) show a similar expansion pattern for the features that are visible in both lines. Remarkably low plane-of-sky velocities of $\leqslant$ 15 km s^{-1} are seen for the [N II]-bright knot complexes immediately north and west of the central star.

5 KINEMATIC COMPONENTS

In order to investigate the kinematics of the nebula in detail, we have measured the velocities of distinct emission components in each slit spectra and organized them into broad systems based on their location, morphology and degree of ionization.

5.1 High-ionization shells

These systems represent the majority of the [O III] emission in the core of the nebula and show a nested elliptical shell morphology. Figure 3 shows the [O III] emission components associated with these shells, as derived from the longslit spectra. Line-of-sight velocities are given with respect to the nominal systemic velocity (40 km s^{-1} heliocentric), separated into negative velocities (left panel) and positive velocities (right panel). The inner "peanut" shells, with a radius of $5''$ to $7''$, are the brightest and are indicated by thick-lined colored ellipses. The edge of the more extended intermediate shell, with a radius of $8''$ to $12''$, is 10 to 100 times fainter than the inner shells and is indicated by thinner dashed ellipses. Additional miscellaneous emission features located in between these shells are indicated by dot-dashed ellipses. Further features that seem to be associated with the low-ionization knots discussed below in § 5.2 are omitted from the figure.

Although the inner shell is irregular in shape, it shows an apparent elongation along PA $\approx 160°$. The intermediate shell is elongated roughly perpendicular to this, along PA $\approx 70°$. In Figure 4 we plot the velocity of each shell component against position along each of these axes, which we denote axis A and axis B. Each component was assigned to only one axis (A or B), according to its location, but this assignment is unavoidably subjective for components near the center, where the two axes cross.

Along axis A a closed velocity ellipse can be seen for the inner shells, with a maximum splitting of ± 22 km s^{-1} close to the central star and velocities close to zero at either end ($\pm 7''$). The pattern is not entirely symmetric, with a slight gradient of ± 3 km s^{-1} along the length, in which the more negative velocities are at the SSE end. The centroid of the ellipse is also shifted by -3.5 km s^{-1} with respect to the systemic velocity.

Along axis B, which is the apparent minor axis of the inner shells ($\pm 5''$), the ellipse is distorted and the gradient is much more pronounced: ± 11 km s^{-1}, with the more negative velocities at the ENE end (large blue circle symbols in lower panel of Fig. 4). Velocity splitting of ± 9 km s^{-1} is seen near both ends, but it is not clear from the [O III] spectra if the ends are closed or open, since none of the [O III] slits are aligned with this axis. However, one of the [N II] slits (slit W) is indeed oriented close to axis B and, although the shells emit only weakly in [N II], the distorted ellipse is clearly closed at the ENE end (large pink triangle symbol in Fig. 4). The situation is not so clear at the WSW end since any [N II] emission from the shell is swamped by brighter emission from the knot complexes. However, the evidence from *HST* imaging suggests that the shell is closed in this direction also.

The intermediate shell along axis B repeats a similar kinematic pattern to the inner shell, but at larger radii. It is represented by dashed ellipses in Figure 3 and small red circle symbols in Figure 4. The gradient (± 9 km s^{-1}) and splitting (± 8 km s^{-1}) are both marginally smaller than for the inner shell. Note that, unlike the inner shells, the intermediate shell is markedly lop-sided, extending $12''$ to the WSW, but only $10''$ to the ENE.

The miscellaneous high-ionization components lie outside the inner shells and show a spoke-like morphology on the *HST* images. It is represented by dot-dashed ellipses in Figure 3 and small green triangle symbols in Figure 4. They do not show any marked kinematic pattern, but are broadly compatible with the velocities of nearby portions of the intermediate shell.

5.2 Low-ionization Knot complexes

Although the

5.3 Outer lobes

5.4 Haloes

6 DISCUSSION

6.1 Flow axes

6.2 Dynamical ages

References

Fisher G. H., Welsch B. T., 2008, in Howe R., Komm R. W., Balasubramaniam K. S., Petrie G. J. D., eds, Astronomical Society of the Pacific Conference Series Vol. 383, Subsurface and Atmospheric Influences on Solar Activity. San Francisco, p. 373

Welsch B. T., Fisher G. H., Abbett W. P., Regnier S., 2004, ApJ, 610, 1148

This paper has been typeset from a TEX/LATEX file prepared by the author.

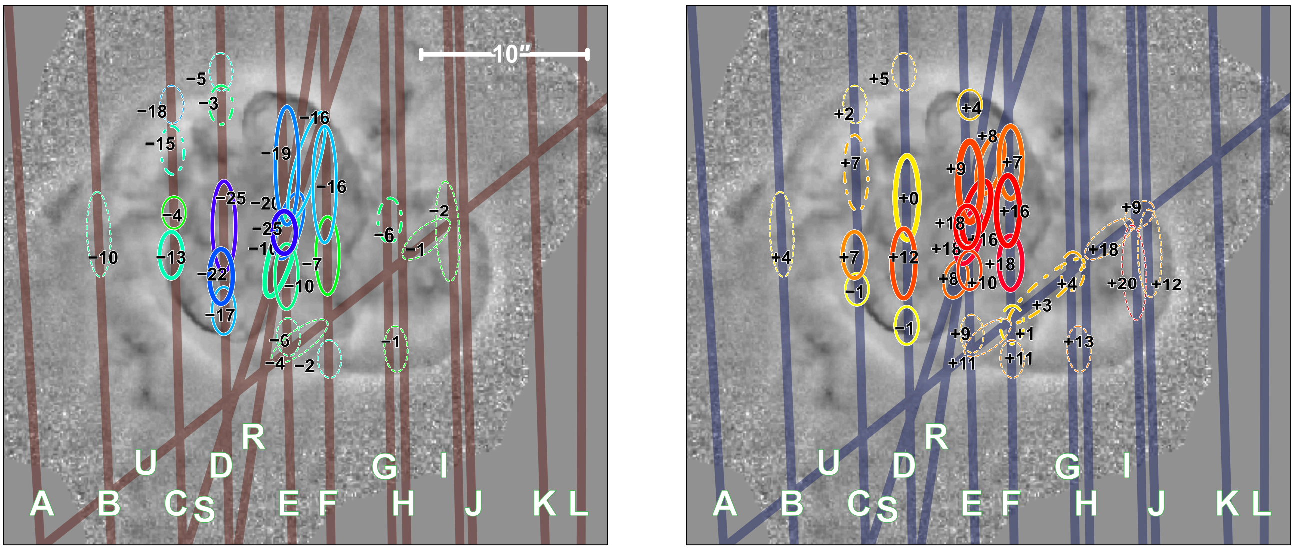

Figure 3. Velocity features in the high-ionization shells, which have been identified in the [O III] slits. Left panel shows blue-shifted features, while right panel shows red-shifted features, each labelled with their line-of-sight velocity with respect to the nominal systemic velocity of 40 km s^{-1}. Solid lines show features in the inner shells, dashed lines show features in the intermediate shell, and dot-dashed lines show miscellaneous features between the two shells. The line width is a qualitative indicator of the brightness of each feature.

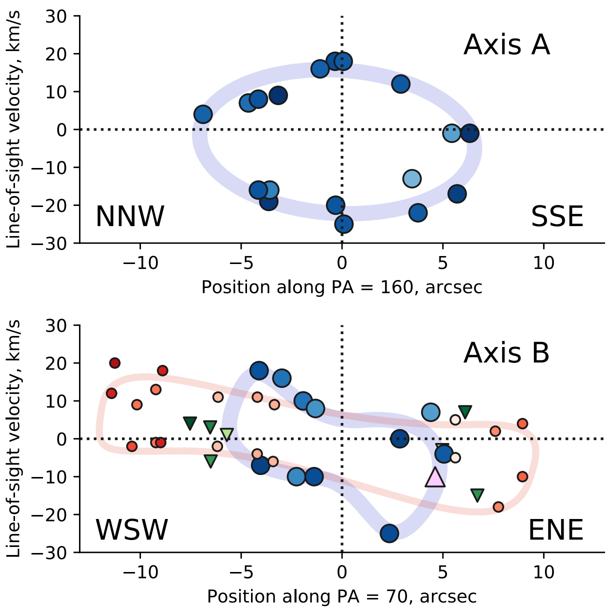

Figure 4. Radial velocity versus position for the shell features shown in Fig. 3. Results are shown along two axes: Axis A (upper panel) is the apparent major projected axis of the inner shells, while Axis B (lower panel) is perpendicular to this. Large blue circles show the inner shell, small red circles show the intermediate shell, and green triangles show miscellaneous features between the two shells. Darker colors indicate features that are closer to each respective axis. Colored lines are merely to guide the eye, and show possible interpretations of the shell kinematics along the two axes.

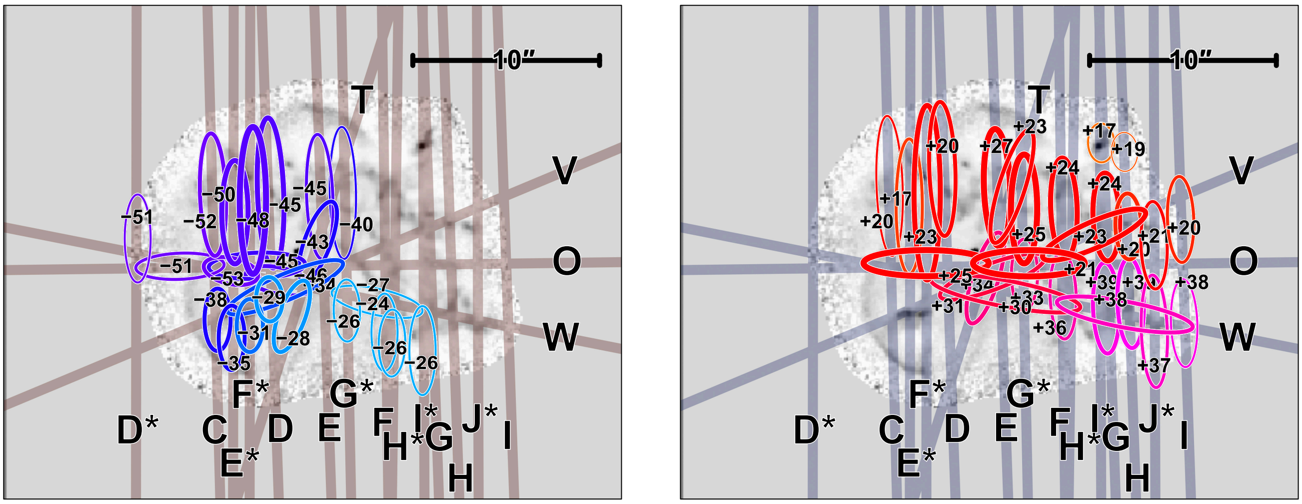

Figure 5. Velocity features in the low-ionization knot complexes, which have been identified in the [N II] slits. Left panel shows blue-shifted features, while right panel shows red-shifted features, each labelled with their line-of-sight velocity with respect to the nominal systemic velocity of 40 km s^{-1}. The line width is a qualitative indicator of the brightness of each feature.

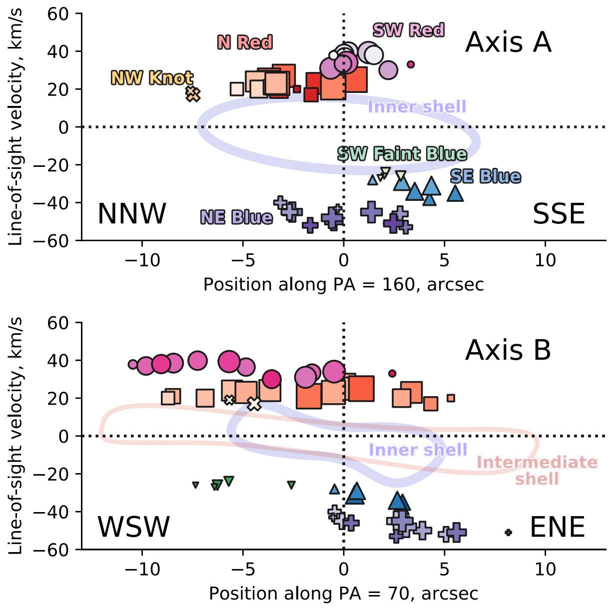

Figure 6. Radial velocity versus position for the low-ionization features features shown in Fig. 5. Results are shown projected along along the same two axes, Axis A (upper panel) and Axis B (lower panel), as in Fig. 4, but this time each feature is shown projected along both axes. The features are divided into 6 different classes, indicated by symbol type and color. Symbol size is proportional to feature brightness (log scale) and symbol shade indicates position along the other axis (darker is more positive). Continuous lines show the same high ionization shells as in Fig. 4.

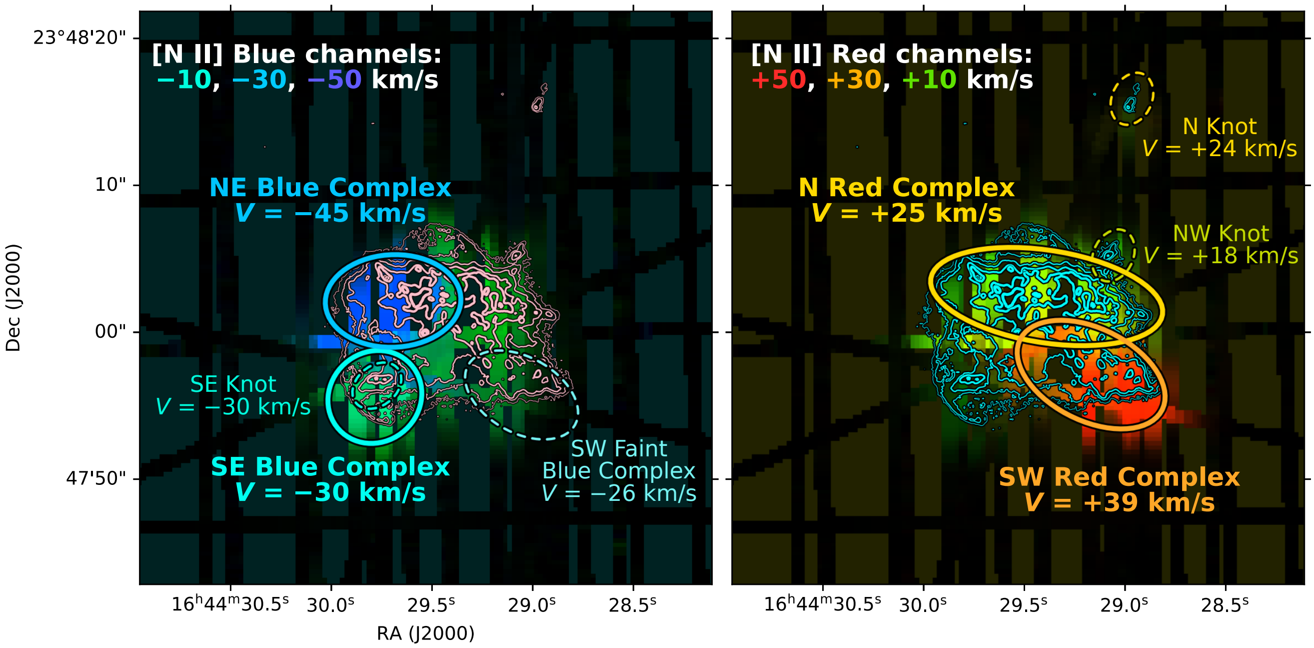

Figure 7. Reconstructed velocity channel maps from the [N II] slit spectra, showing the red-shifted (left panel) and blue-shifted (right panel) knot complexes. Note that channel maps have not been spatially interpolated, so that the individual slit positions can be seen. Each color image is constructed from 3 channels, each of width 20 km s^{-1}, as indicated on the figure. All velocities are with respect to the nominal heliocentric systemic velocity of −40 km s^{-1}.

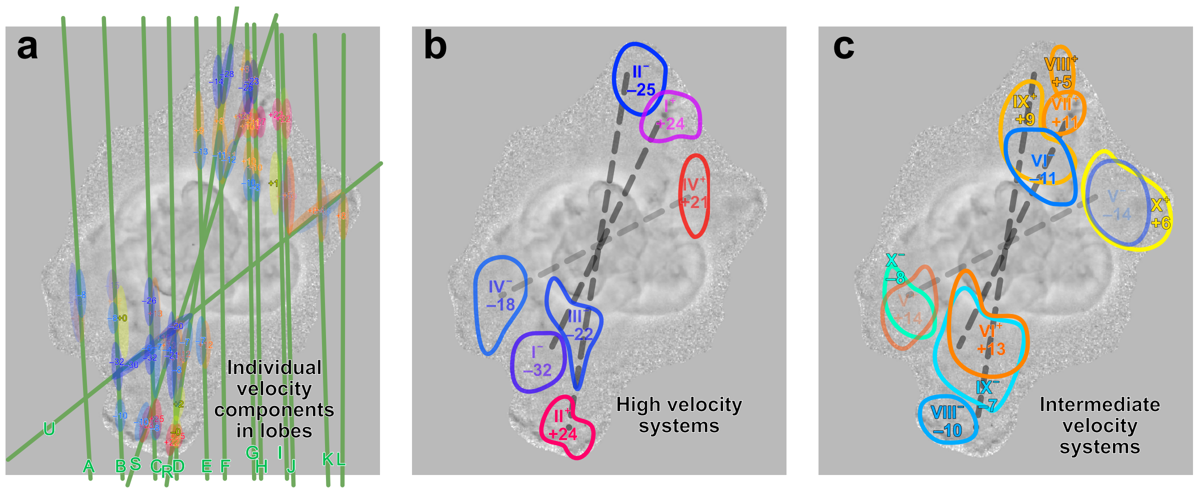

Figure 8. Velocity components and systems in the outer lobes.